Journal of Structural Biology 209 (2020) 107431

Contents lists available at ScienceDirect

Journal of Structural Biology

journal homepage: www.elsevier.com/locate/yjsbi

Coral acid rich protein selects vaterite polymorph *in vitro*

Ra'anan Laipnik[a], Veronica Bissi[b], Chang-Yu Sun[c], Giuseppe Falini[b], Pupa U.P.A. Gilbert[c,d,1], Tali Mass[a,*]

[a] Marine Biology Department, Leon H. Charney School of Marine Sciences, University of Haifa, Israel
[b] Dipartimento di Chimica "Giacomo Ciamician", Università di Bologna, Italy
[c] Department of Physics, University of Wisconsin-Madison, Madison, WI 53706, USA
[d] Departments of Chemistry, Materials Science and Engineering, and Geoscience, University of Wisconsin-Madison, Madison, WI 53706, USA

ARTICLE INFO

Keywords:
Biomineralization
Coral
FTIR
PEEM
XANES
SEM
Protein
Polymorph

ABSTRACT

Corals and other biomineralizing organisms use proteins and other molecules to form different crystalline polymorphs and biomineral structures. In corals, it's been suggested that proteins such as Coral Acid Rich Proteins (CARPs) play a major role in the polymorph selection of their calcium carbonate ($CaCO_3$) aragonite exoskeleton. To date, four CARPs (1–4) have been characterized: each with a different amino acid composition and different temporal and spatial expression patterns during coral developmental stages. Interestingly, CARP3 is able to alter crystallization pathways *in vitro*, yet its function in this process remains enigmatic. To better understand the CARP3 function, we performed two independent *in vitro* $CaCO_3$ polymorph selection experiments using purified recombinant CARP3 at different concentrations and at low or zero Mg^{2+} concentration. Our results show that, in the absence of Mg^{2+}, CARP3 selects for the vaterite polymorph and inhibits calcite. However, in the presence of a low concentration of Mg^{2+} and CARP3 both Mg-calcite and vaterite are formed, with the relative amount of Mg-calcite increasing with CARP3 concentration. In all conditions, CARP3 did not select for the aragonite polymorph, which is the polymorph associated to CARP3 *in vivo*, even in the presence of Mg^{2+} (Mg:Ca molar ratio equal to 1). These results further emphasize the importance of Mg:Ca molar ratios similar to that in seawater (Mg:Ca equal to 5) and the activity of the biological system in a aragonite polymorph selection in coral skeleton formation.

1. Introduction

Biomineralization is a ubiquitous, organic matrix-mediated process in which living organisms control mineral polymorph selection pathways to form complex crystalline structures (Lowenstam, 1981; Weiner and Dove, 2003). It is a process widely found in a range of living organisms across the tree of life, which uses an array of macromolecules for biomineral production (Alvares, 2014; Endo et al., 2004; Fisher et al., 1990; Gu et al., 2000; Mann, 2001; Ritchie et al., 1994; Suzuki et al., 2009). Two major reasons for biomineralization are the production of either endo- or exo-skeletons that can serve as protection or evasion from predation and structural support for tissue. The most abundant biomineral in nature is calcium carbonate ($CaCO_3$) (Lowenstam, 1981; Lowenstam and Weiner, 1989), which can range in size, complexity and polymorphs.

$CaCO_3$ occurs in three crystalline anhydrous polymorphs named calcite, aragonite, and vaterite, yet it can also occur as an amorphous calcium carbonate (ACC) precursor phase which is not considered an actual polymorph (Addadi et al., 2003; Addadi et al., 1995). It can also exist as three hydrated crystalline forms called monohydrocalcite (MHC), ikaite and hemihydrate (Addadi et al., 2003; Mann, 1988; Zou et al., 2019). ACC can also be either hydrated (ACC-H_2O) or dehydrated (ACC) (DeVol et al., 2014; Gong et al., 2012; Politi et al., 2008; Rosas-García et al., 2012) and plays an important precursor role in the biomineralization process (Beniash et al., 1997; Gal et al., 2015). The most common polymorphs of $CaCO_3$ that appear in a variety of marine organisms are aragonite and calcite, though vaterite exists as well (Lowenstam and Abbott, 1975). These polymorphs can begin as an ACC-H_2O and ACC phase *in vivo*, which were first discovered on the surface of fresh sea urchin spicules (Politi et al., 2008) and later in forming sea urchin teeth as well (Killian et al., 2009). In abiotic systems, $CaCO_3$ polymorph selection is mainly governed by temperature, supersaturation, and the presence of other ions such as magnesium (Mg^{2+}) and strontium (Berner, 1975; Ries, 2009). The phase transitions

* Corresponding author.
E-mail address: tmass@univ.haifa.ac.il (T. Mass).
[1] Previously publishing as Gelsomina De Stasio.

https://doi.org/10.1016/j.jsb.2019.107431
Received 6 September 2019; Received in revised form 27 November 2019; Accepted 1 December 2019
Available online 04 December 2019

from ACC-H_2O to ACC to vaterite to aragonite to calcite (not necessarily all present, as phases can be skipped) is an exothermic process, with thermodynamically downhill steps (Radha et al., 2010). Without the intervention of biological mechanisms, these phase transitions in water solutions occur in seconds, whereas with biological control, metastable ACC-H_2O and ACC phases can be kinetically trapped for months inside sea urchin spicules (Gong et al., 2012) or even years in the centers of calcification of corals (DeVol et al., 2015). This kinetic control may, presumably, give marine calcifying organisms the ability to store ACC, and keep it readily available for deposition and crystallization when needed.

Marine calcifying organisms use the resources available in their surroundings to precipitate their $CaCO_3$ structures. Calcium ions (Ca^{2+}) are believed to be transferred from the surrounding waters into the tissue and later transported via vesicles to the calcification sites (Addadi et al., 2006; Beniash et al., 1999; Hayes and Goreau, 1977; Mass et al., 2017; Neder et al., 2019). It is believed that, while the Ca^{2+} ions are transported, they are bound to carbonate ions (CO_3^{2-}) to form stable ACC-H_2O and/or ACC within the vesicles (Beniash et al., 1997). While this process is still enigmatic, research on the sea urchin *P. lividus* has clearly shown vesicles containing ACC particles within the cells that surround the spicule growth compartment (Beniash et al., 1999). Once the ACC particles reach the calcification sites (Beniash et al., 1999), they are then believed to transform into their final crystalline structure. This final crystalline structure formation process has been shown to be under strict biological control in various organisms (DeVol et al., 2015; Von Euw et al., 2017). A variety of $CaCO_3$ biominerals, modern and fossil, even 550-million-year-old *Cloudina* skeletons, have recently been shown to form by attachment of particles, presumably amorphous (Gilbert et al., 2019).

In corals, particles are formed within a tissue called the calicoblastic endothelium, from which skeletal organic matrix (SOM) is secreted to form the aragonite + SOM composite skeletal structure (Tambutté et al., 2011). It is assumed that in the calicoblastic layer, an array of macromolecules including, but not limited to highly acidic proteins (e.g. CARPs), further stabilize and dehydrate ACC-H_2O and ACC and control their crystallization into the final crystal polymorph structures of the coral skeleton (Akiva et al., 2018; Mass et al., 2016; Mass et al., 2017).

The biological mechanism of polymorph selection is still enigmatic, but observations show that distinct proteins derived from the skeletal matrices of sea urchins, corals, and mollusks play a role in the stabilization of ACC-H_2O and ACC or in inhibition of crystal growth (Aizenberg et al., 1996; Akiva et al., 2018; Gong et al., 2012; Kong et al., 2019; Weiner and Addadi, 1997). For example, in corals, distinct CARPs seem to have different roles in the crystallization pathways of the developing coral. Studies show that the Glutamic acid (Glu) rich protein (CARP2) is upregulated prior to settlement, which is a developmental stage associated with ACC. Once calcification of aragonite is initiated post-settlement, Aspartic acid (Asp) rich proteins (CARPs 1, 3, and 4) are up-regulated (Akiva et al., 2018; Mass et al., 2016). Furthermore, proteins derived from the calcareous sponge *Clathrina* and the ascidian tunicate *Pyura pachydermatina* that are rich in Glu, Serine and Glycine (Gly) (Gordon et al., 2003) seem to stabilize ACC (Aizenberg et al., 1996; Weiner and Addadi, 1997), while proteins rich in Asp are associated with the formation of crystalline $CaCO_3$ (Aizenberg et al., 2002; Akiva et al., 2018; Weiner and Addadi, 1997). It has been shown that low poly-Asp concentrations inhibit vaterite formation from ACC and allow calcite polymorph selection *in vitro*, while high poly-Asp concentrations seem to inhibit calcite formation and favor vaterite instead (Zou et al., 2017). Single amino acid moleculea Asp and Glu appear to stabilize clusters of Ca^{2+} and CO_3^{2-} when placed in solution (Picker et al., 2012). This process of stabilization seems to produce clusters of Ca^{2+} and CO_3^{2-} that are poorly dissolved in the solution and therefore are closer to becoming a disordered mineral phase. It is believed that these stabilized clusters are produced through the ionic interactions with the Asp and Glu carboxylic side-chains, yet it seems that full protein structures must play more specific roles in the process (Picker et al., 2012).

So far, four CARPs 1–4 derived from the scleractinian coral *Stylophora pistillata* have been cloned and characterized (Mass et al., 2013). These proteins are localized in different areas within the coral tissue and skeleton, and range in size, acidic amino acid composition, and Asp:Glu ratios, which suggests a different role for each CARP (Mass et al., 2014). The CARP3 molecular weight is 18 kDa, it contains 35% Asp and 15% Glu, has a theoretical isoelectric point pI = 3.04, and is the most acidic of the four CARPs (Mass et al., 2013). It has been shown that CARP3, among other skeletal proteins, is embedded within the aragonite skeleton of the coral and appears to be embedded within the mineral phase of individual skeletal fibers (Mass et al., 2014). Therefore, CARP3 was suggested to have a central role in guiding the specific crystal orientation of the elongated aragonite crystals (Mass et al., 2014). Since CARP3 also has a high percentage of Asp (35%), its function is believed to be associated with the crystallization of $CaCO_3$ (Tobler et al., 2014; Zou et al., 2017).

The exothermic, thermodynamically favored crystallization of $CaCO_3$ in nature (Radha et al., 2010) has been shown to favor the incorporation of Mg^{2+} into the initial phases of crystal formation *in vitro* (Radha et al., 2012; Loste et al., 2003). These phases, as stated above, can begin as ACC, which, when precipitated from Mg-rich solutions, results in Mg-rich ACC *in vitro* (Blue et al., 2017; Loste et al., 2003). Those experiments also show that Mg-rich ACC has a longer lifetime than Mg-poor Mg-poor ACC, and that the lifetime increases with the Mg:Ca molar ratio when precipitated from saturated solutions *in vitro* (Loste et al., 2003). Furthermore, the incorporation of Mg^{2+} into $CaCO_3$ polymorphs to form Mg-calcite, aragonite, and in some cases even $MgCO_3$ can be calculated with classical nucleation theory, provided one takes into account the surface energy of the precipitated particles of these minerals (Sun et al., 2015). The incorporation of Mg^{2+} within $CaCO_3$ structures alters the surface energy of the precipitates. For example, the calculated hydrated surface energy of a pristine nucleus of calcite is 0.21 J/m^2. When compared to the surface energy of aragonite, which is 0.28 J/m^2, it is clear that calcite is the favored precipitate since it is closer to zero. However, once calcite begins incorporating Mg^{2+}, as occurs in modern day seawater conditions, it becomes more soluble, while its surface energy increases to 0.35 J/m^2, making aragonite the more energetically favored precipitate (Sun et al., 2015). It has therefore been suggested that $CaCO_3$ polymorph selection is critically dependent on the aqueous environment conditions, and especially on the Mg:Ca molar ratio (Sun et al., 2015).

Several authors have shown a clear correlation between Mg:Ca molar ratios in the oceans and the abiotically favored polymorph selection of either aragonite or calcite (Berner, 1975; Dickson, 2004; Hardie, 2003). Furthermore, evidence shows that oceanic Mg:Ca molar ratios affect calcifying organisms and the polymorphs they select for their skeletons (Ries, 2009; Ries, 2010). Stanley and Hardie (1998) have shown, from geological records, that marine organisms such as scleractinian corals and calcifying algae shifted their abundance in response to changing Mg:Ca molar ratios over oceanic history. They showed that when the oceanic Mg:Ca molar ratio was > 2 (Middle Paleozoic (400 Ma) through the Early Mesozoic (250 Ma) and from the Cenozoic (60 Ma) to Modern time – i.e. aragonite seas), aragonite and high magnesium calcite were the predominant non-biological precipitates, and aragonite forming organisms seemed to be the dominant reef and sediment producers. When oceanic Mg:Ca molar ratios were < 2 (from the early Paleozoic (525 Ma) and middle to late Mesozoic (240–160 Ma) – i.e. calcite seas), the predominant non-biological precipitate was calcite, and calcite-forming organisms seemed to be the dominant reef and sediment producers. Porter (2007; 2010) showed that mollusk shells that first appeared during an aragonite or calcite sea formed their shell with aragonite or calcite, respectively, and when the ocean conditions fluctuated multiple times between aragonite and

calcite in the last 500 million years, the organisms maintained the original polymorph, rather than adopting the polymorph readily available from seawater.

Two independent studies conducted on recombinant CARP3 have yielded varying results (Gavriel et al., 2018; Mass et al., 2013). Primarily, it is important to mention that even though the recombinant CARP3 described below has not gone through any post-translational modifications, which might be crucial for its function *in vivo*, those experiments clearly demonstrated that CARP3 is able to alter the crystallization pathways of $CaCO_3$ *in vitro*. The first of these two experiments has shown that, when CARP3 is placed in artificial seawater (ASW) with a Mg:Ca molar ratio of ≈ 5.2 (modern day seawater) for two weeks, it precipitates $CaCO_3$ that morphologically resembles aragonite even at pH as low as 7.6 (Mass et al., 2013). The second study tested the function of partial domains of CARP3 or the complete protein in solution with a lower Mg:Ca molar ratio of 2.5. Interestingly, the acidic domain of CARP3 managed to completely shift the polymorph selection of $CaCO_3$ from a mixture of aragonite and high-Mg-calcite towards high-Mg-calcite, whereas both CARP3 or its variable domain, alone, only partially shifted it (Gavriel et al., 2018). Thus, CARP3 clearly plays a role in polymorph selection. The results of these two prior experiments on the possible function of CARP3 are crucial, because (i) the separation of CARP3 from the organic matrix of the coral is currently not possible, and because (ii) the study of single protein function in the biomineralization process is of high importance. Furthermore, the evidence presented by the above two studies is highly suggestive that Mg:Ca molar ratios play a crucial influencing role on CARP3's polymorph selection ability. If that is also the case *in vivo*, it would require a greater attention to magnesium concentrations at different developmental stages in the coral. The recent discovery that Mg-calcite crystals are present in newly formed coral crystals *in vivo* (Neder et al., 2019) may very well depend on the local Mg concentration at the time of mineral deposition. Would a lower Mg:Ca ratio favor the polymorph selection of calcite in the presence of CARP3? What would happen in the absence of any Mg^{2+}? To address these questions, we used both low and zero concentrations of Mg^{2+}, and diverse concentrations of CARP3, in order to understand the role of Mg^{2+} on CARP3-mediated polymorph selection of $CaCO_3$ *in vitro*.

Zero or low Mg concentrations in this study were selected because previous experiments showed that the entire organic matrix extracted from mollusk shells (Belcher et al., 1996; Falini et al., 1996a), or peptides inspired by a nacre protein (Metzler et al., 2010) were able to induce the formation of aragonite from Mg-free solutions. It is therefore possible for proteins to induce the formation of aragonite even in the absence of Mg. Is this the biological function of CARP3, in coral skeleton formation?

2. Materials and methods

2.1. High expression and purification of CARP3

CARP3 was grown in *E. coli* BL21 containing PDEST-17 plasmid and extracted as described in (Mass et al., 2013) with some modifications (Fig. S1A). Briefly, 2% Bacto™ yeast extract was added to the growth medium (Collins et al., 2013). CARP3 was expressed by induction with 0.2% L-Arabinose at OD600 = 1.0 and left 18 h over-night at 18^0C. The 6XHis-tagged CARP3 were purified using the AKTA Avant25 Fast Protein Liquid Chromatography (FPLC) system. First, CARP3 lysate was purified by high affinity nickel column "His-Trap™ Q HP" (GE), followed by secondary purification with a strong anion exchange column "Hi-Trap™ Q HP" (GE) following protocols from Gavriel et al. (2018). A third purification step used a gel filtration column (HiLoad™ 16/600 Superdex™ 75 pg) for size separation and de-salting prior to experimentation. Each purification step fractions were run on SDS-Page 12% to determine best fraction collection for next step (Fig. S1B). Western Blot of all FPLC steps was performed using CARP3 rabbit polyclonal Ab conjugated to goat anti-rabbit (GAR) (Mass et al., 2014) Ab and later reacted with ECL (Fig. S1C).

2.2. Macro-scale polymorph selection of calcium carbonate in the presence of CARP3

2.2.1. Synthesis of $CaCO_3$

For these experiments we used a 30x30x50 cm^3 crystallization chamber containing one 25 ml beaker filled with 3.5 g of $(NH_4)_2CO_3$ (Carlo Erba), covered with parafilm in which ten holes were made. We also had a Petri dish (d = 8 cm) with 16 gr of anhydrous $CaCl_2$ (Fluka) and a 24 well plate used for cell culture (MICROPLATE 24 well with Lid, IWAKI) which contained a round glass coverslip in each well. The round glass cover slips were washed with ethanol and fast dried using an infrared lamp. The wells had a final volume of 750 µL. In the first set of crystallization experiments, in which only calcium chloride was used, each well contained 375 µL of a 20 mM $CaCl_2$ solution, 5-µL of CARP3 solution at a concentration of 0.5 mg/ml and Milli-Q water to volume completion (CARP3 final concentration of 3.33 µg/mL). Once done, the microplate was covered with an aluminum foil and holes were made over every well.

Experiments using both Ca^{2+} and CO_3^{2-} were designed to better simulate the real crystallization conditions in seawater. The solution with the Mg:Ca ratio equal to 1 was prepared filling each well with 188-µL $CaCl_2$ 40 mM, 188-µL $MgCl_2$ 40 mM, same amount of sample used in the first set of experiments and Milli-Q water to completion. The experiment proceeded for four days at room temperature. The obtained crystals were washed three times with Milli-Q water and one time with ethanol before their successive analyses.

2.2.2. Optical microscopy observations

The optical microscope observations of calcium carbonate precipitates were made with a Leica microscope equipped with a digital camera (Moticam 5). The Moticam 5 captures the image through the MI Devices interface and transfers it to the application software (Motic Images Plus 2.0) for further analysis. The camera has a live resolution of 5.0 MP (2592x1944) and 12 mm focusable lenses. Before analysis, samples were washed with water and air dried. Crystals above the glass coverslip were directly observed without extracting the glass coverslip from the microplate. Images were all taken using the 4X magnification, both with polarized and non-polarized light.

2.2.3. Scanning electron microscopy observations

SEM images of uncoated samples were collected by using a Phenom Pro Desktop microscope and applying a tension of 3 kV. The instrument has a light optical magnification range from 20 to 134 X, an electron magnification range from 80 to 15000 X, a resolution of less than 8-nm and a BSD detector. Samples were prepared by breaking the glass coverslip and placing a small fragment on the stub. We used standard 12.5 mm diameter aluminum SEM pin stubs, covered with carbon tabs. After preparation, samples were left inside a desiccator for a couple of hours and then cleaned with compressed air to remove any dust residue.

2.2.4. Fourier-transform infrared spectroscopy (FTIR)

To analyze the product obtained from the crystallization solutions, we used the Thermo Scientific™ Nicolet™ iS™10 FTIR Spectrometer. The instrument has a spectral range from 350 to 7800 cm^{-1} optimized, mid-infrared KBr beam splitter, Mid-infrared Ever-Glo, and a Tungsten/halogen source with resolution better than 0.4 wavenumbers. The instrument is also equipped with an OMNICTM Spectra Software that contains a database of spectral data useful for identifying materials and verifying assumptions. Disk sample for FTIR analysis was obtained by mixing a small amount (< 1 mg) of product with 100 mg of KBr and applying a pressure of 45 tsi (620.5 MPa) to the mixture using a

hydraulic press.

2.3. Nano scale calcium carbonate polymorph selection experiment

We used the calcite wafer assay described by Gong et al., 2012, which consists of depositing a pure CARP3 aqueous solution solution on the surface of a pure geologic calcite crystal wafer. The aqueous sample dissolved some of the $CaCO_3$, which was left to dry and reprecipitate in the presence of CARP3. We then utilized soft x-ray PhotoEmission Electron spectroMicroscopy (PEEM)-X-ray Absorption Near-Edge Structure (XANES) for spectroscopic analysis; we scanned the crystals that were reprecipitated across the calcium L-edge (CaL-edge) and carbon K-edge (CK-edge) and concluded that a less energetically stable polymorph of $CaCO_3$, vaterite, had invariably precipitated in the presence of CARP3 *in vitro*.

2.3.1. Assay for the stabilization of calcium carbonate polymorphs using CARP3 in vitro

Single geologic crystal wafer (MTI Corporation) of calcite (10x10x1mm) was used in the assay. Wafer boundaries coated with 40-nm Pt (Cressington Sputter Coater). 5x1 μL droplets of Mili-Q H_2O and CARP3 sample at 0.1 μg/μL (containing buffers 1.2 mM Bis-Tris and 25 mM NaCl) were deposited consecutively at the center of the wafer approximately every 8.5 min. Once dry, the entire sample including the dried droplet area was coated with 1-nm Pt. A Nikon MM-400 light microscope was used to image the dried sample with an "Infinity 1" camera to map areas of interest for PEEM-XANES analysis. The PEEM-3 microscope at Berkeley Advanced Light Source (ALS) was used to analyze the dried droplets on the calcite wafer to obtain an image and identify the edge of the droplet. Then, a stack of 121 images was acquired across the Ca L-edge and CK-edge (separately) ensuring that every stack contained pixels of both the pure calcite wafer and the edge of the dried droplets for XANES-PEEM analysis.

2.3.2. XANES-PEEM analysis

Spectromicroscopic analysis was done using the PEEM-3 microscope with soft x-ray synchrotron radiation on beamline 11.0.1 at the ALS at the Lawrence Berkeley National Laboratory, California USA. Both Ca L-edge and C K-edge mapping and spectra for the *in vitro* assay of CARP3 protein function were obtained. In both cases, the images had a field of view (FOV) of 56-μm and were comprised of over 10^6 pixels, each containing the full CaL-edge or C K-edge spectrum, each pixel measuring 60 nm in size. Each time the sample was illuminated at a specific photon energy, a 60-μm FOV image was acquired and saved. A total of 121 images were taken, which are referred to as a stack to form each pixel's absorbance spectrum. For calcium, we acquired a stack of 121 images with photon energy across the calcium L-edge from 340 eV to 360 eV (with steps of 0.1 eV between 345 and 355 eV and steps of 0.5 eV for the rest) to later determine the precise $CaCO_3$ polymorph (e.g. calcite, aragonite, vaterite or ACC-H_2O). We also acquired a stack of 145 images of photon energy across the C K-edge from 280 eV to 320 eV (with steps of 0.1 eV between 286 and 294 eV and steps of 0.5 eV for the rest) to detect organic components (e.g. CARP3). Therefore, every pixel in a stack contained the entire Ca L-edge or the C K-edge XANES spectrum each pixel in the analyzed sample area.

See Gong et al. 2012 and Mass et al. 2017 for detailed methods. The radiation dose was kept as small as possible during all PEEM experiments (Parasassi et al., 1991).

2.3.3. Component spectra

All reference spectra, termed component spectra here, were comprised of several averaged single pixel absorption spectra acquired from different polymorphs of calcium carbonate. Reference spectra (Fig. 4D) were obtained from several sources; Aragonite spectra were obtained from DeVol et al., (2014); Calcite spectra were averaged from pixels taken from the wafer sample away from the dried droplet and also compared to DeVol et al., (2014) reference for validation (Fig. 3A). Vaterite spectra were also averaged from single pixels from two separate stacks and validated with DeVol et al., (2014) spectra for peak matching and resulted in a more ordered vaterite structure because peaks 1 and 3 were narrower than in the DeVol reference, and the dip between peaks 1 and 2 was also deeper, thus the peaks were better resolved (Fig. 3B).

2.3.4. Component mapping

Raw data image stacks from the CARP3 function experiment were analyzed using GG Macros for IGOR 6.0 Pro (http://home.physics.wisc.edu/gilbert/). We stacked all images for carbon and calcium separately, which allowed us to obtain full Ca and C spectrum for each pixel in each stack. For Ca L-edge, we let the software calculate which linear combination of component spectra best fit the spectrum from each pixel, using calcite, vaterite, and aragonite as component spectra. We then mapped the spatial distribution of the three component spectra as an RGB map (Fig. 4C), where Red = aragonite, Green = vaterite, and Blue = calcite) for each sample area analyzed. Since some pixels did not contain sufficient Ca intensity for spectral analysis, they were masked off from the RGB map and appear as black pixels. In addition, the red pixels representing aragonite were regarded as noise and do not represent aragonite.

To normalize C K-edge spectra, we acquired the Izero from the thick 40-nm Pt area on the wafer. C spectra were obtained by extracting spectra from each pixel along the lines indicated in Fig. 5A, binned 7, thus not acquiring single-pixels, but each time averaging the 49 spectra from a 7-pixel square. The spectra from each 7-pixel square from each line were then plotted, aligned in energy and intensity, and averaged. The average spectra from each of the 3 lines were then again plotted, aligned in energy and intensity, and averaged. The resulting spectra for calcite and CARP3 droplet, along with the Izero averaged spectrum, were then plotted in Fig. 5B, used for component mapping in Fig. 5C and normalized to the Izero in Fig. 5D. Izero spectra were extracted and averaged similarly. The calcite and CARP3 droplet averaged C spectra were normalized to the Izero spectrum by simply dividing the former by the latter. Once normalized, spectra from the CARP3 droplet showed the characteristic peaks associated with carboxyl (C═O) bonds in polypeptide chains at 288 eV, and the carbonate peak at 290.3 eV associated with all carbonates. The carbonate peak was observed on the calcite substrate, and also on the CARP3 droplet (Fig. 5D) (Brandes et al., 2004).

3. Results

3.1. Macro-scale polymorph selection of calcium carbonate in the presence of CARP3

3.1.1. SEM and FTIR spectroscopy analysis

This experiment aimed to evaluate the effect of CARP3 on the morphology and polymorphism of $CaCO_3$ formed from a 10 mM $CaCl_2$ solution or a 10 mM $CaCl_2$ plus 10 mM $MgCl_2$ solution in which vapors from $(NH_4)_2CO_3$ diffused into a closed system (Kontrec et al., 2008). This experimental setup requires a high volume of solution. Therefore, we were limited by the amount of CARP3 that we could use. In addition, the Fourier Transform Infra Red (FTIR) spectroscopy measurements require a minimum of about 1 mg of mineral for detection.

Control experiments, carried out in the absence of CARP3, showed that from the Ca^{2+} solution, single crystals exhibiting the typical rhombohedral {10.4} shape of calcite were formed. This was shown by optical microscope (OM) (Figs. S2A & S3A) and SEM images (Fig. 1A). Calcite was confirmed by the analysis of the FTIR spectrum (Fig. 2A) which showed absorption bands of calcite at 1422 cm^{-1} (ν_3), 875 cm^{-1} (ν_2) and 712 cm^{-1} (ν_4) (Whittaker, 1975). Together with calcite crystals, a few spherical particles were observed by SEM as well. They showed the typical shape and morphology of vaterite (Fig. 1C), but

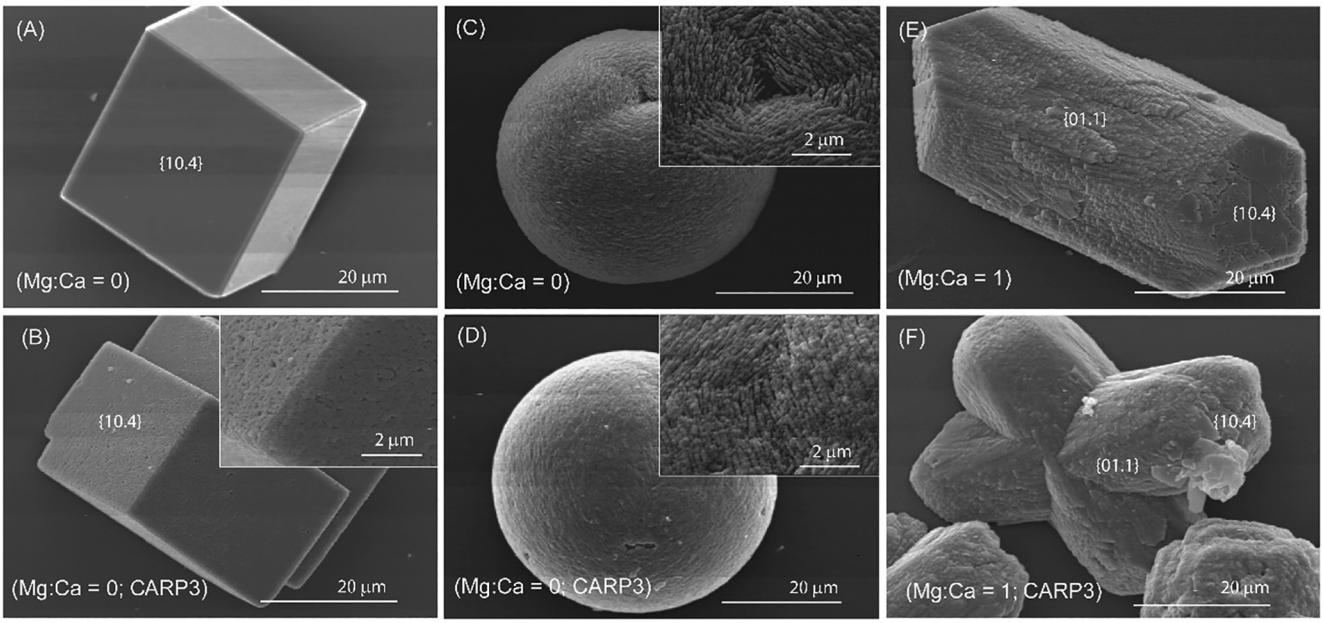

Fig. 1. SEM images of $CaCO_3$ formed from a $CaCl_2$ solution (A, B, C, D) in the absence (A, C) and in the presence (B, D) of 3.33 µg/mL CARP3. (E, F) SEM images of $CaCO_3$ formed from a molar ratio Mg:Ca = 1 solution, in the absence (E) and in the presence of CARP3 (F). The crystal morphology suggests calcite in A and B, vaterite in C and D, and Mg-calcite in E and F. Each crystal is representative of its entire population.

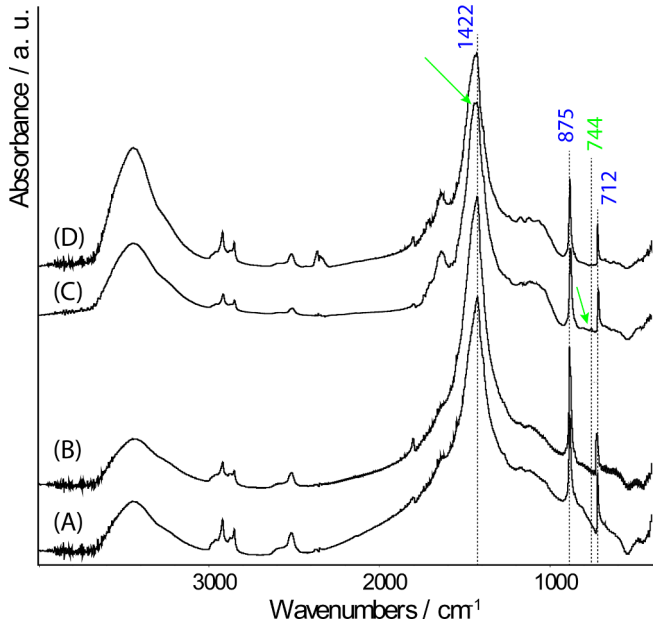

Fig. 2. FTIR spectra (labeled as the samples in Fig. 1) of calcium carbonate formed from a $CaCl_2$ solution in the absence (A) and presence of 3.33 µg/mL CARP3 (B). (E, F) FTIR spectra of $CaCO_3$ precipitated from a molar ratio Mg:Ca = 1 solution without (E) and with CARP3 (F). The typical absorption bands of calcite at 1422 cm^{-1} (ν_3), 875 cm^{-1} (ν_2) and 712 cm^{-1} (ν_4) were detected and suggested a low content of Mg^{2+} within the crystal lattice of calcite. They are marked by blue wavenumbers. The presence of vaterite is detected by the ν_4 band at 744 cm^{-1} (green wavenumber) and the broadening of the ν_3 band at about 1430 cm^{-1} (indicated by the green arrows). Extensive vaterite as in Fig. 1C and 1D was not detectable in the transmission FTIR experiment thus no spectra C and D are presented. (For interpretation of the references to color in this figure legend, the reader is referred to the web version of this article.)

their absorption bands were not detected in the FTIR spectrum (Fig. 2A). The crystals formed from the solution containing Mg^{2+} and Ca^{2+} with Mg:Ca molar ratio equal to 1, exhibited the morphology of single crystals of Mg-calcite (Fig. 1E, S2B & S3B), which appeared elongated along the c-axis and expressed additional pseudo {01.1} faces together with the typical rhombohedral {10.4} ones (Fig. 1E) (Falini et al., 1996a). The FTIR spectrum in Fig. 2E showed absorption bands at 1422 cm^{-1} (ν_3), 875 cm^{-1} (ν_2) and 712 cm^{-1} (ν_4) which were the same of those of calcite, suggesting a very low content of Mg^{2+} within the lattice of calcite (Fig. 2E) (Falini et al., 1996a). In this condition the formation of vaterite-like spherical particles was not observed and vaterite absorption bands were not detected by the FTIR spectroscopy (Fig. 2E).

When 3.33 µg/mL CARP3 was present in the $CaCl_2$ crystallization solution, the polymorph selection of $CaCO_3$ was affected with respect to the control experiment. Calcite was still observed, but a higher relative amount (not quantified) of vaterite was detected. This higher concentration of vaterite was revealed by the presence of a higher density of spherical particles in the OM and SEM images (Fig. S2&S3) and by the analysis of the FTIR spectrum (Fig. 2B), where a weak additional absorption band at 744 cm^{-1} and a broadening on the ν_3 bands to higher wavenumbers were observed (Whittaker, 1975). OM and SEM images showed that calcite crystals still appeared as perfect rhombohedra that in some cases were interpenetrated (Figs. S2C & S3C). However, the presence of CARP3 induced surface roughness on the calcite crystals (Fig. 1B), and a more compact, less porous texture of the vaterite aggregated crystallites (Fig. 1D) with respect to the control (Fig. 1C). When CARP3 was present in the Mg:Ca = 1 solution the OM and SEM observations showed only the presence of crystals having the morphology of Mg-calcite and the absence of vaterite-like spherical particles (Fig. 1F, S2B & S3B). This polymorph selection of Mg-calcite was still observed in the FTIR spectrum, where no vaterite absorption bands were revealed (Fig. 2F). The crystals of Mg-calcite showed a rougher {10.4} surface (Fig. 1F), with respect to those formed in the absence of CARP3 (Fig. 1E, S2B & S3B).

3.2. Nano-scale polymorph selection of calcium carbonate in the presence of CARP3

3.2.1. Ca L-edge spectroscopy analysis and component mapping

Next, we wanted to check the effect of high concentrations of CARP3 on the $CaCO_3$ polymorph selection pathway. For that, we had to

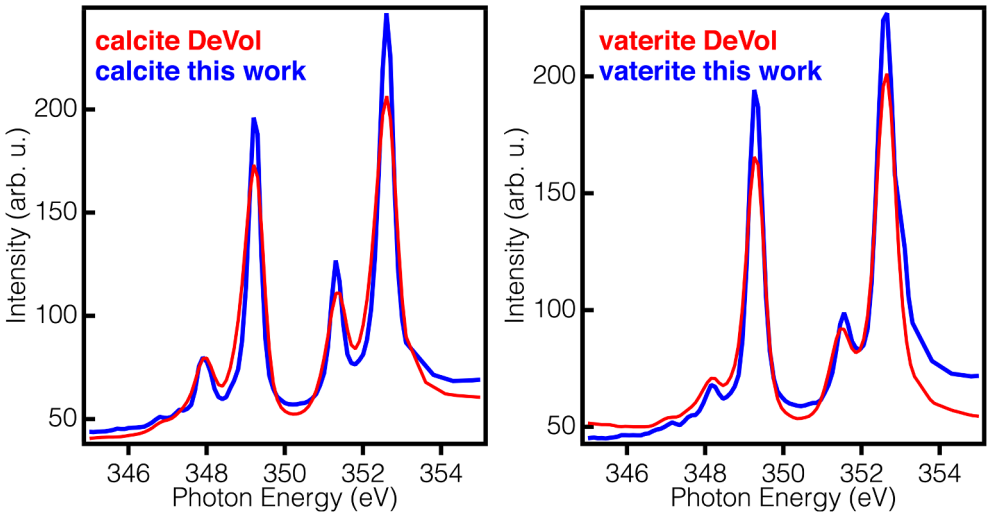

Fig. 3. Comparison of DeVol et al. (2014) reference spectra and averaged spectra from the present samples for (A) calcite wafer and (B) CARP3-templated vaterite. The absorption spectra in the present work indicate a more ordered crystal structure, based on better resolved (lower dip between) peaks 1 & 2 and peaks 3 & 4 in both A and B. The excellent agreement of the present spectra with the DeVol et al. (2014) references confirms the assignment of the CARP3-induced mineral to vaterite. Minor differences are observed in peak intensities but not in peak positions. The minor peak intensity difference are due to the use of a different diffraction grating in the beamline.

use PEEM-XANES spectroscopy, a much more sensitive technique that measures a layer of mineral as thin as 3-nm (Frazer et al., 2003). The signal for such a thin layer of mineral cannot be detected by microscopic vibration spectroscopic techniques (Whittaker, 1975). We placed five consecutive 1 μL droplets of CARP3 at 100 μg/mL concentration, on a single-crystalline calcite wafer, let them air-dry before depositing the next droplet on top of the previous one, and analyzed the dried droplet by Ca L-edge PEEM-XANES spectroscopy as described by Gong et al., (2012). The dry droplet on the calcite wafer (Fig. 4A) had a clearly visible droplet boundary and had plentiful crystalline structures. We zoomed in using PEEM on an area of interest (Fig. 4B) containing both the calcite wafer and the edge of the dried droplet for XANES spectroscopy. We obtained reference absorption spectra from DeVol et al., (2014), which were acquired on the same beamline but with a different monochromator grating, thus after comparison to absorption spectra acquired from the present sample, we decided to use the present

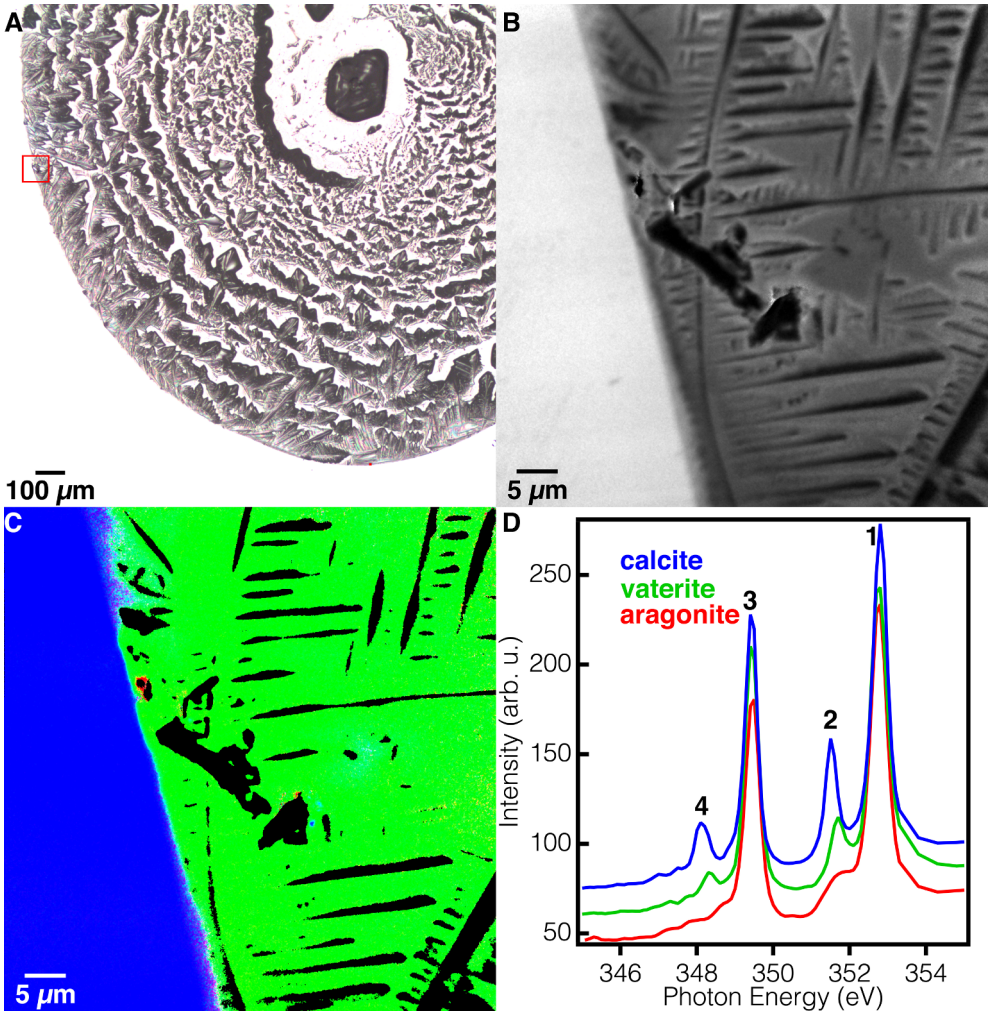

Fig. 4. Ca L-edge XANES spectromicroscopy of CARP3 droplet and calcite wafer to assay CARP3 function in polymorph selection. (A) Visible light microscopy image of the dried droplet on the calcite wafer. The red box indicates the area magnified in B and C. (B) PEEM image of the area in the red box in A. The crystals abundant in the droplet are salts from the buffer, and they appear morphologically but not chemically, as they are partly coated with vaterite, and PEEM imaging and spectra are only sensitive to the top ~3 nm of the surface. (C) RGB component map obtained with PEEM of the same area in B, where the color of each pixel displays the concentration of each mineral: Red = aragonite, Green = vaterite, Blue = Calcite. The black pixels were masked off based on insufficient Ca intensity for spectral analysis. These crystals must have not been coated with vaterite. The few red pixels are not aragonite, they fall in the noise category. (D) Ca L-edge XANES spectra used as components in C, correspondingly colored. Notice that the spectral line-shapes are similar for calcite and vaterite, but the energy positions of peaks 2 and 4 (labeled with black numbers) are different, thus they can be distinguished and mapped, as in C.

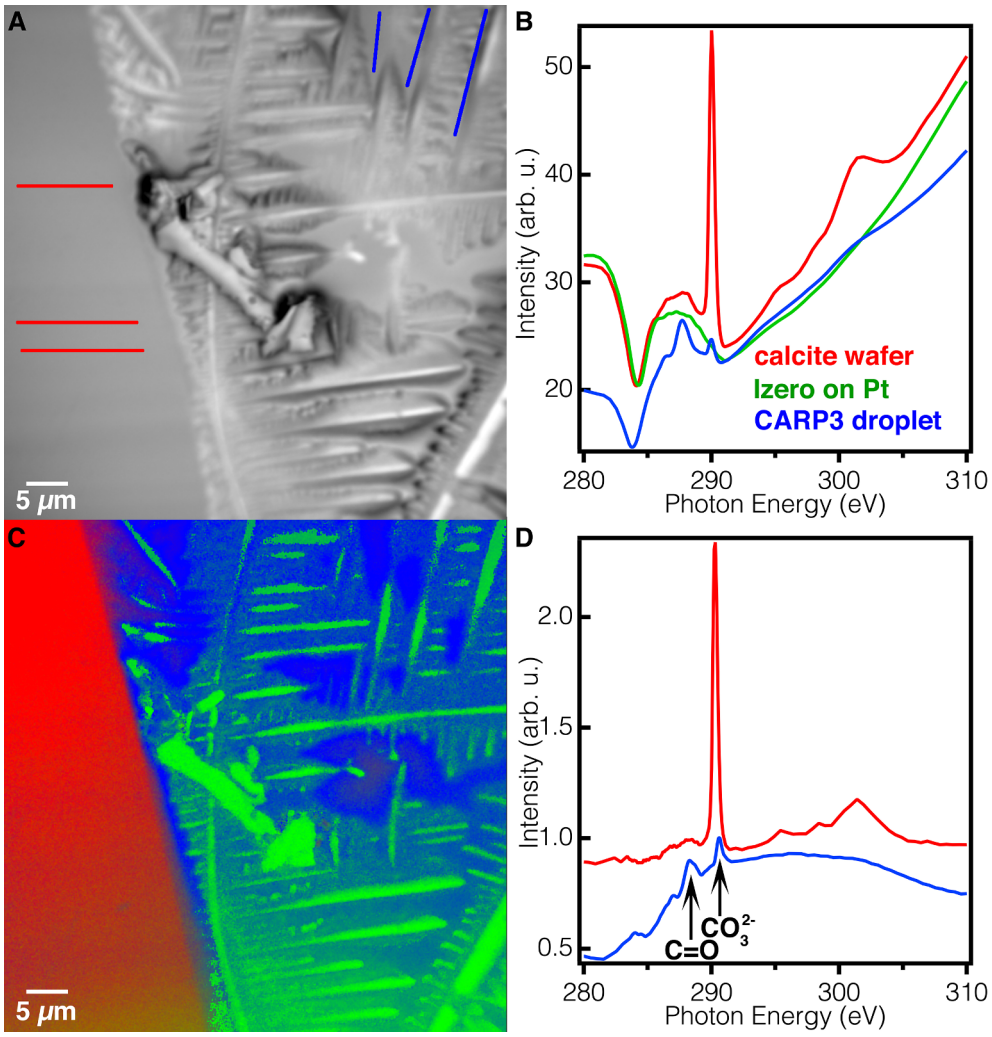

Fig. 5. C K-edge XANES spectra of CARP3 droplet and calcite wafer to test the presence CARP3 and its intact peptide bonds. (A) PEEM image of the droplet edge region analyzed, indicating the lines along which C K-edge spectra were extracted. Red lines: calcite wafer, Blue lines: carbon-rich CARP3 droplet areas. (B) Raw absorption spectra from the colored lines in A, with the same color labeling, in addition to the beamline Izero curve (Green) used for component mapping and spectra normalization. The CARP3 spectrum is displaced vertically for clarity. (C) Component mapping of same sample region obtained using the component spectra in B. (D) Absorption spectra normalized to the Izero, revealing a clear peak at 290.3 eV, characteristic of all carbonates, present in both substrate and droplet regions, and a peak at ~288.2 eV, characteristic of the carboxyl groups (C═O) in each peptide bond (Boese et al., 1997; Brandes et al., 2004; Gordon et al., 2003; Myers et al., 2018), and thus indicative of protein presence. This peak is only observed in the dried droplet, and not on the calcite substrate. Again, here the proteins are on top of the salt crystals. The latter appear green because their spectra are exactly identical to the beamline Izero, that is, they contain no carbon on their surfaces.

calcite and vaterite absorption spectra as component spectra (Fig. 3) for component mapping.

We then analyzed the 10^6 pixels in the image with component mapping, that is, found the best fit to-each pixel spectrum with a linear combination of the three component spectra displayed in Fig. 4D. Assigning each component spectrum an RGB color, as shown in Fig. 4D we obtained the RGB component map presented in Fig. 4C. Of all possible $CaCO_3$ polymorphs we observed only vaterite where the droplet had dried. The masked off pixels (Black) did not contain sufficient Ca intensity for spectral analysis and the pixels representing aragonite (Red) were also unreliable and fall under the noise category. We also observed pure calcite on all the surrounding calcite wafer, as expected. The unexpected result was to observe so much vaterite everywhere in the dried CARP3 droplet, and no aragonite, calcite, or Mg-calcite at all.

3.2.2. C K-Edge spectroscopy analysis

In order to verify that the dissolved Ca^{2+} and CO_3^{2-} had re-precipitated as vaterite in the presence of CARP3, and that CARP3 and vaterite were co-localized everywhere in the droplet, we analyzed the same region at the carbon K-edge. The XANES spectra extracted from specific blue or red lines in the CARP3 droplet or calcite wafer. (Fig. 5A) revealed two distinct spectra (Fig. 5B) plotted in blue and red. We then performed component mapping (Fig. 5C) on the entire sample using the spectra in Fig. 5B as components with the addition of the beamline background (Izero) spectrum (Fig. 5B Green) as a third reference for component mapping in RGB colors. The results revealed a clear localization distinction between the two spectra, which coincides with the boundary between the dried droplet and the calcite wafer (Fig. 5C). After normalization to the Izero (Fig. S4A & S4B) presented in Fig. 5D, we found that the calcite wafer (red region) site showed a sharp peak at 290.3 eV (Fig. 5D), as expected, because this peak is characteristic of all carbonates. The vaterite-rich droplet region (blue) showed a clear peak at 288.2 eV consistent with the carboxyl (C═O) groups in peptide bonds, along with a carbonate peak at 290.3 eV (Brandes et al., 2004). These results indicate that the re-precipitation of the Ca^{2+} and CO_3^{2-} indeed occurred in the presence of CARP3. The similar intensities of the carbonate peak and the peptide bond peak indicate that the droplet surface (~3 nm) contained approximately the same amount of proteins and vaterite, within one order of magnitude.

4. Discussion

In this study, we focused on further understanding the *in vitro* biochemical function of the recombinant CARP3 derived from the widely studied stony coral *S. pistillata*. *S. pistillata*, through the process of biomineralization, utilizes an array of macromolecules, including the highly acidic CARPs to precipitate its $CaCO_3$ exo-skeleton as the aragonite polymorph (Mass et al., 2014; Tambutté et al., 2011). In order to understand CARP3 function in the biomineralization process *in vivo*, it is important to extend the investigation on how a low concentration of Mg^{2+} affects CARP3 calcification activity *in vitro* and therefore might be used by the coral during the course of its development to achieve polymorph selection. Since CARP3 is rich in Asp and is derived from an aragonite-producing organism, prior research (Mass et al., 2013; Picker

et al., 2012; Tobler et al., 2014) suggests that it is more likely to precipitate aragonite than to stabilize ACC-H_2O or ACC. Here, we found that in solutions lacking Mg^{2+}, both low and high concentrations of CARP3 seem to either alter or hinder the polymorph selection of calcite and favor vaterite instead. Furthermore, it appears that the polymorph selection of vaterite is concentration dependent where the higher the CARP3 concentration, the more vaterite is formed. A similar effect was observed for a 40 kDa protein extracted from the mollusk *Strombus decorus persicus*, associated with biogenic aragonite polymorph selection. When the 40 kDa protein was added to a solution of $CaCO_3$ the only $CaCO_3$ polymorph detected was vaterite (Pokroy et al., 2006). While this study is focused on a single CARP protein, it is important to remember that the CARP3 protein is found *in vivo* among a vast number of micro- and macro-molecules in the coralline tissue and SOM.

Independent research and polymorph selection experiments conducted by various groups (Goffredo et al., 2011; Hohn and Reymond, 2019; Marin et al., 1996; Njegić Džakula et al., 2019; Raz et al., 2003) on the effects of SOM & coral mucus (CM) on the polymorph selection of $CaCO_3$ *in vitro* produced varying results and suggestions. One group has suggested that the organic molecules within the SOM are derived from early CM and act as inhibitors of calcification (Marin et al., 1996). Furthermore, polymorph selection experiments on fragments of coral skeletons in the presence of SOM or CM, separately, do not seem to change the precipitation rates of $CaCO_3$. These results were the same even when Mg^{2+} was present in oversaturated $CaCO_3$ solutions. However, SOM and CM do seem to influence the primary polymorph selection (Hohn and Reymond, 2019). It was therefore suggested that the SOM molecules do not change the kinetics of polymorph selection, but rather influence the formation of one specific polymorph (Hohn and Reymond, 2019). One group studying the sea urchin *Strongylocentrotus purpuratus* had shown that the organic matrix, extracted from spicules at two developmental stages, has a temporal function variance. They suggest that even though the extracted proteins from the spicules at 48- and 72-hours post-fertilization (hpf) are similar, they induce different crystallization outcomes. At 48 hpf the extracted molecules promote the formation of ACC, whereas at 72 hpf, the extracted molecules promote the formation of calcite (Raz et al., 2003).

Further independent experiments showed that SOMs extracted from mollusk shells (Belcher et al., 1996; Falini et al., 1996b) or peptides inspired by a nacre protein (Metzler et al., 2010) were able to induce the formation of aragonite from Mg-free solutions. Other experiments (Reggi et al., 2014) showed that the SOMs extracted from several species of coral skeletons generally do not induce the formation of aragonite at low Mg:Ca molar ratios. Yet, the acidic macromolecules extracted from the *Balanophyllia europaea* coral did favor the co-formation of calcite and aragonite in the absence of Mg^{2+} (Reggi et al., 2014). The experimental data reported in this paper show that CARP3 affects polymorph selection, both in the absence of Mg and with a Mg:Ca ratio of 1. This observation can add information on how Mg^{2+} affects the different stages of the biomineralization process in corals interacting with mineralizing proteins, differently from what is known about acidic macromolecules extracted from mollusks, where Mg^{2+} are not necessary for the formation of aragonite. In addition, the fact that the majority of extracted acidic macromolecules from coral do not favor the precipitation of aragonite, hints at the possibility that even though the recombinant CARP3 has not gone through any post-translational modifications, it still resembles the results obtained from these previous experiments. These previous *in vitro* works that studied the entire SOM had the advantage of representing the majority of the intracrystalline SOM. However, they did not describe the role of individual macromolecules and their activity. Since CARP3 has been shown to be upregulated in the post settlement stage associated with the formation of aragonite (Akiva et al., 2018; Mass et al., 2016), the question of what polymorph would be selected, should it be placed in a solution containing either no Mg^{2+} at all or a Mg:Ca ratio of 1 arose. The previous results emphasize the importance of single protein function experiments such as this one. Especially, since this one specific protein, CARP3, is the only one experimentally proven to be intracrystalline in corals (Gavriel et al., 2018).

The crystals formed in our large-volume, low-CARP3 concentration experiments, using solutions containing only $CaCl_2$ and $MgCl_2$ with molar ratio Mg:Ca of 1, shared the same polymorph and morphology with their controls, respectively. The reason for choosing a Mg:Ca molar ratio of 1 is that, in the absence of additives, it leads to the polymorph selection of only Mg-calcite. Therefore, under this condition, the ability of an additive (e.g. CARP3) to select a polymorph can be easily tested. At higher Mg:Ca molar ratio, Mg-calcite and aragonite usually co-precipitate.

We observed a minimal (using $CaCl_2$ solution) or no (using Mg:Ca 1 solutions) polymorph or shape variance of $CaCO_3$ particles between experiments at low CARP3 concentration and no-CARP3 controls. However, the interaction between the crystals and CARP3 was quite evident once the SEM images (Fig. 1) revealed that calcite and Mg-calcite crystals grown in the presence of CARP3 had a porous, uneven surface, which was absent from the controls. These findings suggest that CARP3 was interacting with the surface layers of these crystals. The formation of this uneven surface can be attributed to the fact that the adsorbed CARP3 onto the growing calcite, or Mg-calcite, surface is much larger than the crystal lattice of calcite (a few Å). CARP3 proteins behave as inclusions in the crystal. Thus, the advancing calcite growth front can engulf the proteins that are eventually incorporated into the crystalline bulk (Sear, 2012; Tambutté et al., 2011). Even before the incorporation, the flat surfaces of {10.4} rhombohedra may be perturbed by the presence of these foreign objects, which may change fluid dynamics, local supersaturation and, consequently, introduce morphological changes to the growing crystal surfaces.

Vaterite was only present in the Mg^{2+} deficient experiment results, and its concentration was increased by the presence of CARP3 such that it could be detected by FTIR. Thus, to some extent, CARP3 inhibited the polymorph selection of calcite and favored that of vaterite instead. At low concentration, CARP3 seems to interact with vaterite, as observed for calcite, promoting the aggregation of vaterite crystallites, while at high concentration, it seems to promote a thin layer of interspersed CARP3 and vaterite. A previous study (Zou et al., 2017) has shown a correlation between the addition of low concentrations of poly-Asp (pAsp) and the inhibition of vaterite polymorph formation from ACC. In our chemical systems the supersaturation is gradually increased as the vapors from ammonium carbonate diffuse into the solutions (low CARP3 concentration experiments) or droplet evaporates (high CARP3 concentration experiments), and the formation of vaterite is not, presumably, from ACC. One hundred percent vaterite was precipitated when using the high concentration (100 μg/mL) of CARP3 and a lower, FTIR detectable, amount of vaterite was also precipitated with a low CARP3 concentration (3.33 μg/mL) (Fig. 1D&2B). Zou et al.'s experiment tested concentrations of pAsp between 0 and 12 % that showed a concentration-dependent effect of pAsp. They showed that at low concentration (0–3%) pAsp inhibits vaterite, whereas at high concentration (6–12%) pAsp promotes vaterite formation. In our experiment a much lower concentration of CARP3 (0.00033%) was used and yet, vaterite formed, albeit in a small amount. This different behavior of a protein (CARP3) compared to a polypeptide (pAsp) is expected and has its origin in the different folding and amino acid sequence specificity that characterize protein from biominerals, even while taking into account that this particular recombinant protein (CARP3) has not gone through any post-translational modifications. Indeed, just to cite an example, a concentration of 0.0005% of a protein extracted from the mollusk shell of *S. decorus persicus* induced the formation of vaterite in amounts detectable by X-ray diffraction (Pokroy et al., 2006).

When Mg^{2+} ions were present in solution, no vaterite or aragonite formed, only Mg-calcite crystals. The fact that no aragonite formed was probably due to the low Mg:Ca molar ratio of 1, despite the presence of CARP3, which was previously associated with aragonite formation,

from seawater (Mass et al., 2013). Thermodynamic tests and calculations show a minimum Mg:Ca molar ratio requirement of 2–2.5 for aragonite polymorph selection (Sun et al., 2015). Loste et al. (2003) have also shown that formation of crystals via ACC *in vitro* favors the incorporation of magnesium into the crystalline structure. Picker et al. (2012) have shown that not only do Asp and Glu stabilize clusters of Ca^{2+} and CO_3^{2-} in solution (Picker et al., 2012), but when magnesium is added at increasing Mg:Ca ratios, it seems to favor the incorporation of magnesium into ACC at increasing concentration *in vitro*. In addition, it seems that carboxylic acids in general have the tendency to favor magnesium incorporation into ACC (Wang et al., 2009).

In prior experiments using CARP3's acidic domain, which is rich in Asp (≈62%) and placed in a solution with Mg:Ca molar ratio of 2.5, a full polymorph selection shift occurred towards Mg-calcite (Gavriel et al., 2018). These observations may suggest that certain acidic proteins in the biomineralization world might interact with Mg^{2+} for the initial precipitation of the ACC phase and thus lower the ΔG required for $CaCO_3$ crystallization (Wang et al., 2009). The abundance and location of different calcification-associated proteins might be linked to magnesium-incorporation into the skeletal structure (Meibom et al., 2004).

Once we increased the concentration of CARP3 to 100 μg/mL (≈100 ppm) and gradually, further increased the concentration as the droplet evaporated in our second and independent polymorph-selection experiment without magnesium, all of the precipitated mineral was vaterite (Fig. 4C). The fact that all of the precipitated $CaCO_3$ crystals were vaterite is consistent with Asp-rich proteins' function in crystallization and polymorph selection, rather than stabilization of ACC-H_2O or ACC. We note that in a previous droplet assay experiment by Gong et al. 2012 with a variety of proteins in the droplet, only calcite precipitated, with the notable exception of the sea urchin skeletal matrix protein SM50, which precipitated stable ACC-H_2O (Gong et al., 2012). This protein is highly alkaline – pI (pH ~ 12.9) (Veis, 2011), rich in Gly (NP_999775.1) and, compared to controls (H_2O, cdk1, PPL A2, BSA) it appeared to be the only inhibitor of crystallization pathways to calcite, and stabilized ACC-H_2O *in vitro*. In the spicule, ACC-H_2O was stable up to 2 months post-mortem. Combined, the CARP3 and SM50 experiments suggest a strong influence by these proteins on $CaCO_3$ polymorph selection. The CARP3 experiment, in addition, emphasizes the influence of magnesium on the templated $CaCO_3$ polymorph.

The fact that CARP3 does not induce the formation of aragonite at low or zero concentration of Mg is relevant to understanding the natural biomineralization process: It demonstrates that in corals the involvement of acidic macromolecules in polymorph selection is completely different from that observed in mollusks (Belcher et al., 1996; Falini et al., 1996a; Metzler et al., 2010), where magnesium ions are irrelevant to aragonite formation. In coral high Mg and CARP3 are both necessary for aragonite formation.

5. Conclusion

Two independent polymorph selection experiments have shown here that in the absence of Mg CARP3 inhibits the formation of calcite and selects for the vaterite polymorph only. In the presence of Mg, with Mg:Ca = 1, both vaterite and Mg-calcite are formed, with the proportion of Mg-calcite increasing with the CARP3 concentration. Aragonite was never observed, in any of the experimental conditions, indicating that greater Mg:Ca ratios are necessary for aragonite formation, which differs from the *in vitro* effect mollusk proteins. These results indicating that CARP3 modifies the $CaCO_3$ crystallization pathway but is not able to precipitate aragonite without the presence of high Mg:Ca molar ratios, or a preassembled aragonite structure. Finally, we believe that the CARP3 polymorph selection of vaterite in the absence of Mg^{2+} further strengthens the paramount importance that these ions play in polymorph selection during the $CaCO_3$ biomineralization process.

Author contributions

T.M., G.F and P.U.P.A.G. designed research; R.L., V.B., C.-Y.S., G.F., P.U.P.A.G. and T.M., performed research; R.L., V.B., C.-Y.S., G.F., and P.U.P.A.G. analyzed data; and R.L., G.F., P.U.P.A.G. and T.M wrote the paper.

Declaration of Competing Interest

The authors declare that they have no known competing financial interests or personal relationships that could have appeared to influence the work reported in this paper.

Acknowledgments

We would like to thank Ricardo Almuly for lab work instruction and support; Meirav Avital-Shacham from University of Haifa at Human Biology Department for use and instruction of FPLC systems; TM acknowledges support from the European Research Council (ERC; Grant # 755876) and the Israel Science Foundation, Israel (Grant # 312/15). PG acknowledges support from the U.S. Department of Energy, Office of Science, Office of Basic Energy Sciences, Chemical Sciences, Geosciences, and Biosciences Division, under Award DE-FG02-07ER15899, and NSF grant DMR-1603192. PEEM experiments were done on beamline 11.0.1.1 at the Advanced Light Source, which is supported by the Director, Office of Science, Office of Basic Energy Sciences, of the U.S. Department of Energy under Contract No. DE-AC02-05CH11231.

Appendix A. Supplementary data

Supplementary data to this article can be found online at https://doi.org/10.1016/j.jsb.2019.107431.

References

Addadi, L., Raz, S., Weiner, S., 2003. Taking advantage of disorder: amorphous calcium carbonate and its roles in biomineralization. Adv. Mater. 15, 959–970.
Addadi, L., Joester, D., Nudelman, F., Weiner, S., 2006. Mollusk shell formation: a source of new concepts for understanding biomineralization processes. Chemistry 12, 980–987.
Addadi, L., Aizenberg, J., Albeck, S., Falini, G., Weiner, S., 1995. Structural control over the formation of calcium carbonate mineral phases in biomineralization, p. 127-139, Supramolecular stereochemistry, Springer.
Aizenberg, J., Addadi, L., Weiner, S., Lambert, G., 1996. Stabilization of amorphous calcium carbonate by specialized macromolecules in biological and synthetic precipitates. Adv. Mater. 8, 222–226.
Aizenberg, J., Lambert, G., Weiner, S., Addadi, L., 2002. Factors involved in the formation of amorphous and crystalline calcium carbonate: a study of an ascidian skeleton. J. Am. Chem. Soc. 124, 32–39.
Akiva, A., Neder, M., Kahil, K., Gavriel, R., Pinkas, I., Goobes, G., Mass, T., 2018. Minerals in the pre-settled coral Stylophora pistillata crystallize via protein and ion changes. Nat. Commun. 9, 1880.
Alvares, K., 2014. The role of acidic phosphoproteins in biomineralization. Connect. Tissue Res. 55, 34–40.
Belcher, A.M., Wu, X., Christensen, R., Hansma, P., Stucky, G., Morse, D., 1996. Control of crystal phase switching and orientation by soluble mollusc-shell proteins. Nature 381, 56.
Beniash, E., Addadi, L., Weiner, S., 1999. Cellular control over spicule formation in sea urchin embryos: a structural approach. J. Struct. Biol. 125, 50–62.
Beniash, E., Aizenberg, J., Addadi, L., Weiner, S., 1997. Amorphous calcium carbonate transforms into calcite during sea urchin larval spicule growth. Proc. R. Soc. Lond. B Biol. Sci. 264, 461–465.
Berner, R., 1975. The role of magnesium in the crystal growth of calcite and aragonite from sea water. Geochim. Cosmochim. Acta 39, 489–504.
Blue, C.R., Giuffre, A., Mergelsberg, S., Han, N., De Yoreo, J.J., Dove, P.M., 2017. Chemical and physical controls on the transformation of amorphous calcium carbonate into crystalline $CaCO_3$ polymorphs. Geochim. Cosmochim. Acta 196, 179–196.
Boese, J., Osanna, A., Jacobsen, C., Kirz, J., 1997. Carbon edge XANES spectroscopy of amino acids and peptides. J. Electron Spectrosc. Relat. Phenom. 85, 9–15.
Brandes, J.A., Lee, C., Wakeham, S., Peterson, M., Jacobsen, C., Wirick, S., Cody, G., 2004. Examining marine particulate organic matter at sub-micron scales using scanning transmission X-ray microscopy and carbon X-ray absorption near edge structure spectroscopy. Mar. Chem. 92, 107–121.
Collins, T., Azevedo-Silva, J., da Costa, A., Branca, F., Machado, R., Casal, M., 2013. Batch

production of a silk-elastin-like protein in E. coli BL21 (DE3): key parameters for optimisation. Microb. Cell Fact. 12, 21.
DeVol, R.T., Sun, C.Y., Marcus, M.A., Coppersmith, S.N., Myneni, S.C., Gilbert, P.U., 2015. Nanoscale transforming mineral phases in fresh nacre. J. Am. Chem. Soc. 137, 13325–13333.
DeVol, R.T., Metzler, R.A., Kabalah-Amitai, L., Pokroy, B., Politi, Y., Gal, A., Addadi, L., Weiner, S., Fernandez-Martinez, A., Demichelis, R., Gale, J.D., Ihli, J., Meldrum, F.C., Blonsky, A.Z., Killian, C.E., Salling, C.B., Young, A.T., Marcus, M.A., Scholl, A., Doran, A., Jenkins, C., Bechtel, H.A., Gilbert, P.U., 2014. Oxygen spectroscopy and polarization-dependent imaging contrast (PIC)-mapping of calcium carbonate minerals and biominerals. J. Phys. Chem. B 118, 8449–8457.
Dickson, J., 2004. Echinoderm skeletal preservation: calcite-aragonite seas and the Mg/Ca ratio of Phanerozoic oceans. J. Sediment. Res. 74, 355–365.
Endo, H., Takagi, Y., Ozaki, N., Kogure, T., Watanabe, T., 2004. A crustacean Ca^{2+}-binding protein with a glutamate-rich sequence promotes CaCO3 crystallization. Biochem J 384, 159–167.
Falini, G., Gazzano, M., Ripamonti, A., 1996a. Magnesium calcite crystallizatin from water–alcohol mixtures. Chem. Commun. 1037–1038.
Falini, G., Albeck, S., Weiner, S., Addadi, L., 1996b. Control of aragonite or calcite polymorphism by mollusk shell macromolecules. Science 271, 67–69.
Fisher, L.W., McBride, O.W., Termine, J.D., Young, M.F., 1990. Human bone sialoprotein. Deduced protein sequence and chromosomal localization. J. Biol. Chem. 265, 2347–2351.
Frazer, B.H., Gilbert, B., Sonderegger, B.R., De Stasio, G., 2003. The probing depth of total electron yield in the sub-keV range: TEY-XAS and X-PEEM. Surf. Sci. 537, 161–167.
Gal, A., Weiner, S., Addadi, L., 2015. A perspective on underlying crystal growth mechanisms in biomineralization: solution mediated growth versus nanosphere particle accretion. CrystEngComm 17, 2606–2615.
Gavriel, R., Nadav-Tsubery, M., Glick, Y., Yarmolenko, A., Kofman, R., Keinan-Adamsky, K., Berman, A., Mass, T., Goobes, G., 2018. The coral protein CARP3 acts from a disordered mineral surface film to divert aragonite crystallization in favor of Mg-calcite. Adv. Funct. Mater. 28, 1707321.
Gilbert, P., Porter, S.M., Sun, C.Y., Xiao, S., Gibson, B.M., Shenkar, N., Knoll, A.H., 2019. Biomineralization by particle attachment in early animals. Proc. Natl. Acad. Sci. U.S.A. 116, 17659–17665.
Goffredo, S., Vergni, P., Reggi, M., Caroselli, E., Sparla, F., Levy, O., Dubinsky, Z., Falini, G., 2011. The skeletal organic matrix from Mediterranean coral *Balanophyllia europaea* influences calcium carbonate precipitation. PLoS ONE 6, e22338.
Gong, Y.U., Killian, C.E., Olson, I.C., Appathurai, N.P., Amasino, A.L., Martin, M.C., Holt, L.J., Wilt, F.H., Gilbert, P.U., 2012. Phase transitions in biogenic amorphous calcium carbonate. Proc. Natl. Acad. Sci. U.S.A. 109, 6088–6093.
Gordon, M.L., Cooper, G., Morin, C., Araki, T., Turci, C.C., Kaznatcheev, K., Hitchcock, A.P., 2003. Inner-shell excitation spectroscopy of the peptide bond: Comparison of the C 1s, N 1s, and O 1s spectra of glycine, glycyl-glycine, and glycyl-glycyl-glycine. J. Phys. Chem. A 107, 6144–6159.
Gu, K., Chang, S., Ritchie, H.H., Clarkson, B.H., Rutherford, R.B., 2000. Molecular cloning of a human dentin sialophosphoprotein gene. Eur. J. Oral Sci. 108, 35–42.
Hardie, L.A., 2003. Secular variations in Precambrian seawater chemistry and the timing of Precambrian aragonite seas and calcite seas. Geology 31, 785–788.
Hayes, R.L., Goreau, N.I., 1977. Intracellular crystal-bearing vesicles in the epidermis of scleractinian corals, *Astrangia danae* (Agassiz) and *Porites porites* (Pallas). Biol. Bull. 152, 26–40.
Hohn, S., Reymond, C.E., 2019. Coral calcification, mucus, and the origin of skeletal organic molecules. Coral Reefs 38, 973–984.
Killian, C.E., Metzler, R.A., Gong, Y.U., Olson, I.C., Aizenberg, J., Politi, Y., Wilt, F.H., Scholl, A., Young, A., Doran, A., Kunz, M., Tamura, N., Coppersmith, S.N., Gilbert, P.U., 2009. Mechanism of calcite co-orientation in the sea urchin tooth. J. Am. Chem. Soc. 131, 18404–18409.
Kong, J., Liu, C., Yang, D., Yan, Y., Chen, Y., Liu, Y., Zheng, G., Xie, L., Zhang, R., 2019. A novel basic matrix protein of *Pinctada fucata*, PNU9, functions as inhibitor during crystallization of aragonite. CrystEngComm 21, 1250–1261.
Kontrec, J., Kralj, D., Brečević, L., Falini, G., 2008. Influence of some polysaccharides on the production of calcium carbonate filler particles. J. Cryst. Growth 310, 4554–4560.
Loste, E., Wilson, R.M., Seshadri, R., Meldrum, F.C., 2003. The role of magnesium in stabilising amorphous calcium carbonate and controlling calcite morphologies. J. Cryst. Growth 254, 206–218.
Lowenstam, H.A., 1981. Minerals formed by organisms. Science 211, 1126–1131.
Lowenstam, H.A., Abbott, D.P., 1975. Vaterite: a mineralization product of the hard tissues of a marine organism (Ascidiacea). Science 188, 363–365.
Lowenstam, H.A., Weiner, S., 1989. On biomineralization Oxford University Press, New York.
Mann, S., 1988. Molecular recognition in biomineralization. Nature 332, 119–124.
Mann, S., 2001. Biomineralization: Principles and Concepts in Bioinorganic Materials Chemistry Oxford University Press, New York.
Marin, F., Smith, M., Isa, Y., Muyzer, G., Westbroek, P., 1996. Skeletal matrices, muci, and the origin of invertebrate calcification. Proc. Natl. Acad. Sci. U.S.A. 93, 1554–1559.
Mass, T., Drake, J.L., Peters, E.C., Jiang, W., Falkowski, P.G., 2014. Immunolocalization of skeletal matrix proteins in tissue and mineral of the coral *Stylophora pistillata*. Proc. Natl. Acad. Sci. U.S.A. 111, 12728–12733.
Mass, T., Drake, J.L., Haramaty, L., Kim, J.D., Zelzion, E., Bhattacharya, D., Falkowski, P.G., 2013. Cloning and characterization of four novel coral acid-rich proteins that precipitate carbonates in vitro. Curr. Biol. 23, 1126–1131.
Mass, T., Putnam, H.M., Drake, J.L., Zelzion, E., Gates, R.D., Bhattacharya, D., Falkowski, P.G., 2016. Temporal and spatial expression patterns of biomineralization proteins during early development in the stony coral *Pocillopora damicornis*. Proc. Biol. Sci. 283.
Mass, T., Giuffre, A.J., Sun, C.Y., Stifler, C.A., Frazier, M.J., Neder, M., Tamura, N., Stan, C.V., Marcus, M.A., Gilbert, P., 2017. Amorphous calcium carbonate particles form coral skeletons. Proc. Natl. Acad. Sci. U.S.A. 114, E7670–E7678.
Meibom, A., Cuif, J.P., Hillion, F., Constantz, B.R., Juillet-Leclerc, A., Dauphin, Y., Watanabe, T., Dunbar, R.B., 2004. Distribution of magnesium in coral skeleton. Geophys. Res. Lett. 31.
Metzler, R.A., Evans, J.S., Killian, C.E., Zhou, D., Churchill, T.H., Appathurai, N.P., Coppersmith, S.N., Gilbert, P.U., 2010. Nacre protein fragment templates lamellar aragonite growth. J. Am. Chem. Soc. 132, 6329–6334.
Myers, C.E., Bergmann, K.D., Sun, C.-Y., Boekelheide, N., Knoll, A.H., Gilbert, P.U., 2018. Exceptional preservation of organic matrix and shell microstructure in a Late Cretaceous Pinna fossil revealed by photoemission electron spectromicroscopy. Geology 46, 711–714.
Neder, M., Laissue, P.P., Akiva, A., Akkaynak, D., Alberic, M., Spaeker, O., Politi, Y., Pinkas, I., Mass, T., 2019. Mineral formation in the primary polyps of pocilloporoid corals. Acta Biomater. 96, 631–645.
Njegić Džakula, B., Fermani, S., Dubinsky, Z., Goffredo, S., Falini, G., Kralj, D., 2019. In vitro coral biomineralization under relevant aragonite supersaturation conditions. Chem. Eur. J. 25, 10616–10624.
Parasassi, T., Sapora, O., Giusti, A.M., De Stasio, G., Ravagnan, G., 1991. Alterations in erythrocyte membrane lipids induced by low doses of ionizing radiation as revealed by 1,6-diphenyl-1,3,5-hexatriene fluorescence lifetime. Int. J. Radiat. Biol. 59, 59–69.
Picker, A., Kellermeier, M., Seto, J., Gebauer, D., Cölfen, H., 2012. The multiple effects of amino acids on the early stages of calcium carbonate crystallization. Zeitschrift für Kristallographie-Crystalline Mater. 227, 744–757.
Pokroy, B., Zolotoyabko, E., Adir, N., 2006. Purification and functional analysis of a 40 kD protein extracted from the *Strombus decorus persicus* mollusk shells. Biomacromolecules 7, 550–556.
Politi, Y., Metzler, R.A., Abrecht, M., Gilbert, B., Wilt, F.H., Sagi, I., Addadi, L., Weiner, S., Gilbert, P.U., 2008. Transformation mechanism of amorphous calcium carbonate into calcite in the sea urchin larval spicule. Proc. Natl. Acad. Sci. U.S.A. 105, 17362–17366.
Porter, S.M., 2007. Seawater chemistry and early carbonate biomineralization. Science 316, 1302.
Porter, S.M., 2010. Calcite and aragonite seas and the de novo acquisition of carbonate skeletons. Geobiology 8, 256–277.
Radha, A., Forbes, T.Z., Killian, C.E., Gilbert, P., Navrotsky, A., 2010. Transformation and crystallization energetics of synthetic and biogenic amorphous calcium carbonate. Proc. Natl. Acad. Sci. 107, 16438–16443.
Radha, A.V., Fernandez-Martinez, A., Hu, Y., Jun, Y.-S., Waychunas, G.A., Navrotsky, A., 2012. Navrotsky, Energetic and structural studies of amorphous $Ca1-xMgxCO_3{\cdot}nH_2O$ ($0 \leqslant x \leqslant 1$). Geochim. Cosmochim. Acta. 90, 83–95.
Raz, S., Hamilton, P.C., Wilt, F.H., Weiner, S., Addadi, L., 2003. The transient phase of amorphous calcium carbonate in sea urchin larval spicules: the involvement of proteins and magnesium ions in its formation and stabilization. Adv. Funct. Mater. 13, 480–486.
Reggi, M., Fermani, S., Landi, V., Sparla, F., Caroselli, E., Gizzi, F., Dubinsky, Z., Levy, O., Cuif, J.-P., Dauphin, Y., 2014. Biomineralization in Mediterranean corals: the role of the intraskeletal organic matrix. Cryst. Growth Des. 14, 4310–4320.
Ries, J., 2009. The effects of secular variation in seawater Mg/Ca on marine biocalcification. Biogeosciences Discussions 6.
Ries, J.B., 2010. Geological and experimental evidence for secular variation in seawater Mg/Ca (calcite-aragonite seas) and its effects on marine biological calcification. Biogeosciences 7, 2795–2849.
Ritchie, H.H., Hou, H., Veis, A., Butler, W.T., 1994. Cloning and sequence determination of rat dentin sialoprotein, a novel dentin protein. J. Biol. Chem. 269, 3698–3702.
Rosas-García, V.M., del Carmen Sáenz-Tavera, I., Cantú-Morales, D.E., 2012. Onset of amorphous structure in $CaCO_3$: geometric and electronic structures of $(CaCO_3)$ n (n = 2–7) clusters by ab initio calculations. J. Cluster Sci. 23, 203–219.
Sear, R.P., 2012. The non-classical nucleation of crystals: microscopic mechanisms and applications to molecular crystals, ice and calcium carbonate. Int. Mater. Rev. 57, 328–356.
Stanley, S.M., Hardie, L.A., 1998. Secular oscillations in the carbonate mineralogy of reef-building and sediment-producing organisms driven by tectonically forced shifts in seawater chemistry. Palaeogeogr. Palaeoclimatol. Palaeoecol. 144, 3–19.
Sun, W., Jayaraman, S., Chen, W., Persson, K.A., Ceder, G., 2015. Nucleation of metastable aragonite $CaCO_3$ in seawater. Proc. Natl. Acad. Sci. U.S.A. 112, 3199–3204.
Suzuki, M., Saruwatari, K., Kogure, T., Yamamoto, Y., Nishimura, T., Kato, T., Nagasawa, H., 2009. An acidic matrix protein, Pif, is a key macromolecule for nacre formation. Science 325, 1388–1390.
Tambutté, S., Holcomb, M., Ferrier-Pagès, C., Reynaud, S., Tambutté, É., Zoccola, D., Allemand, D., 2011. Coral biomineralization: from the gene to the environment. J. Exp. Mar. Biol. Ecol. 408, 58–78.
Tobler, D.J., Blanco, J.R., Dideriksen, K., Sand, K.K., Bovet, N., Benning, L., Stipp, S.L.S., 2014. The effect of aspartic acid and glycine on amorphous calcium carbonate (ACC) structure, stability and crystallization. Procedia Earth Planet. Sci. 10, 143–148.
Veis, A., 2011. Organic matrix-related mineralization of sea urchin spicules, spines, test and teeth. Front. Biosci. (Landmark Ed.) 16, 2540–2560.
Von Euw, S., Zhang, Q., Manichev, V., Murali, N., Gross, J., Feldman, L.C., Gustafsson, T., Flach, C., Mendelsohn, R., Falkowski, P.G., 2017. Biological control of aragonite formation in stony corals. Science 356, 933–938.
Wang, D., Wallace, A.F., De Yoreo, J.J., Dove, P.M., 2009. Carboxylated molecules regulate magnesium content of amorphous calcium carbonates during calcification. Proc. Natl. Acad. Sci. U.S.A. 106, 21511–21516.

Weiner, S., Addadi, L., 1997. Design strategies in mineralized biological materials. J. Mater. Chem. 7, 689–702.
Weiner, S., Dove, P.M., 2003. An overview of biomineralization processes and the problem of the vital effect. Rev. Mineral. Geochem. 54, 1–29.
Whittaker, E.J.W., 1975. The Infrared Spectra of Minerals, p. 104-104, in: v. c. Farmer, (Ed.), Mineralogical Magazine, Cambridge University Press, London.
Zou, Z., Bertinetti, L., Politi, Y., Fratzl, P., Habraken, W., 2017. Control of polymorph selection in amorphous calcium carbonate crystallization by poly(aspartic acid): two different mechanisms. Small 13.
Zou, Z., Habraken, W., Matveeva, G., Jensen, A.C.S., Bertinetti, L., Hood, M.A., Sun, C.Y., Gilbert, P., Polishchuk, I., Pokroy, B., Mahamid, J., Politi, Y., Weiner, S., Werner, P., Bette, S., Dinnebier, R., Kolb, U., Zolotoyabko, E., Fratzl, P., 2019. A hydrated crystalline calcium carbonate phase: calcium carbonate hemihydrate. Science 363, 396–400.